Molecular Structure of a Fibrillar Alzheimer's Aβ Fragment[†]

Louise C. Serpell,*[,‡] Colin C. F. Blake,[§] and Paul E. Fraser[||]

Neurobiology division, MRC Centre, Laboratory of Molecular Biology, Hills Road, Cambridge CB2 2QH, England U.K, Laboratory of Molecular Biophysics, University of Oxford, Rex Richards Building, South Parks Road, Oxford OX1 3QT, England U.K, and Centre for Research into Neurodegenerative Diseases, and Department of Medical Biophysics, Tanz Neuroscience Building, 6 Queens Park Crescent W, Toronto, Ontario M5S 3H2, Canada

Received March 20, 2000; Revised Manuscript Received August 21, 2000

ABSTRACT: Amyloid-β (Aβ) peptide deposition as fibrillar senile plaques is a key element in the pathology of Alzheimer's disease. Here we present a high-resolution structure of an Aβ amyloid fibril using magnetically aligned preparations of a central Aβ domain which forms representative amyloid fibrils. Diffraction analysis of these samples revealed Bragg reflections on layer lines consistent with a preferred orientation, as opposed to the typical symmetry associated with fibers. These crystalline properties permitted a molecular replacement approach based upon a β-hairpin motif resulting in a structure of the fibrillar Aβ peptide. This detailed molecular structure of Aβ in its fibrous state provides clues as to the mechanism of amyloid assembly and identifies potential targets for controlling the aggregation process.

Alzheimer's disease is characterized by the presence of extracellular and cerebrovascular senile plaques composed of amyloid and by the intraneuronal deposition of neurofibrillary tangles. Amyloid plaques are composed of the Amyloid-β peptide (Aβ),[1] a 39−42 residue fragment that is processed from the larger integral membrane, amyloid precursor protein (APP) (*1*). Aβ is known to play a central role in Alzheimer's disease development, since all known forms of inherited AD are associated with changes in Aβ processing and production (*2*). There are three genes known to be associated with familial AD, APP, presenilin 1, and presenilin 2, and in each of these, APP processing is altered, resulting in an increase in the more amyloidogenic Aβ peptide, Aβ42. Furthermore, Aβ amyloid fibrils have been shown to be neurotoxic in a number of studies (*3*−*5*) suggesting that they play a direct role in neurodegeneration.

Amyloid fibrils in AD and other related disorders are insoluble, ordered aggregates of normally soluble proteins. The fibrils are 70−100 Å in diameter, and these in turn are thought to be composed of several protofilaments (*6*−*8*) (Figure 1). Each protofilament consists of an arrangement of contiguous β-sheet polypeptide chains, which are aligned perpendicular to the long axis of the fiber. These should not be confused with "protofibrils" previously described (*9*, *10*), which constitute semifibrillar aggregates observed in early stages of the amyloid pathway. The protofilaments have

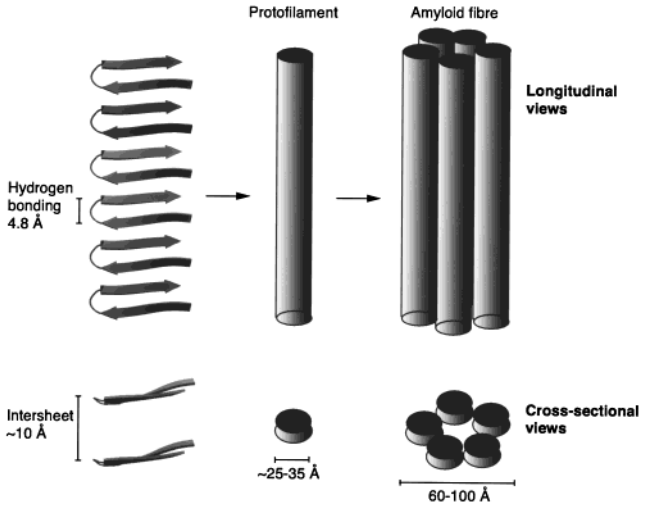

FIGURE 1: Schematic diagram showing the different levels of structure, from the continuous, hydrogen-bonded β-sheet within a protofilament to the organization of the protofilaments in the amyloid fibril.

similar β-sheet organization, but may show differences in their number and dimensions in individual amyloids (*6*, *48*).

Structural studies of ex-vivo amyloid fibrils from Alzheimer's disease brain have provided insights into the organization of the fibril; however, high-resolution data has been limited due to the extreme insolubility of the plaques. Synthetic fragments corresponding to regions of the Aβ peptide have been shown to form amyloid fibrils spontaneously in vitro (*8*, *11*). These fibrils are indistinguishable from tissue amyloid by electron microscopy and exhibit the characteristics of ex-vivo amyloid, such as green birefringence under cross-polarized light when stained with Congo red. However, even synthetic amyloid fibrils are problematic to study using conventional structural techniques. Methods such as single crystal X-ray crystallography and nuclear magnetic resonance

[†] L.C.S. is funded by the Medical Research Council, U.K. P.E.F. acknowledges the support of the Ontario Mental Health Foundation, Alzheimer Association of Ontario, Scottish Rite Charitable Foundation and the Medical Research Council of Canada.

* To whom correspondence should be addressed. Phone: +44 1223 402411. Fax: +44 1223 402310. E-mail: serpell@mrc-lmb.cam.ac.uk.

[‡] Laboratory of Molecular Biology.

[§] Laboratory of Molecular Biophysics.

[||] Centre for Research into Neurodegenerative Diseases.

[1] Abbreviations: Aβ, amyloid β; APP, amyloid precursor protein; AD, Alzheimer's disease; NMR, nuclear magnetic resonance.

10.1021/bi000637v CCC: $19.00 Published 2000 by the American Chemical Society
Published on Web 10/06/2000

(NMR) cannot be used due to the polymer-like nature and insolubility of the fibrils. The conformation and assembly of the Aβ peptide has been studied using a range of biophysical techniques including circular dichroism, Fourier transform infrared spectroscopy, electron microscopy, and X-ray fiber diffraction. These studies have revealed a common theme in which the soluble full length or fragments of peptide have been converted from an α-helical structure or random coil structure to a β-structure upon aggregation (*12*, *13*). The structure of the soluble peptide in organic solvents has been described using 2D NMR (*14*−*16*), which suggests random coil conformation except for two α-helices between residues 15−23 and 31−35 (*14*). These studies are important for understanding the preamyloid state of Aβ to examine the process of amyloid formation, but do not provide information about the aggregated, pathogenic form of Aβ.

Fiber diffraction studies have shown that the Aβ in its fibril form is a predominantly β-sheet conformation (*7*, *8*, *17*−*19*) and exhibits the characteristic X-ray pattern first described for cross-β silk (*20*). It is generally agreed that the β-strands are arranged perpendicular to the fiber axis and this is indicated by a very strong 4.7−4.8 Å reflection on the meridian of X-ray diffraction patterns (*7*, *8*, *18*, *21*, *22*). Fiber diffraction images from magnetically aligned fragments of the Aβ peptide (*18*, *19*) have been obtained, leading to a model of β-sheet crystallites arranged in a pentagonal or hexagonal array. This arrangement has also been suggested for fibrils formed from a fragment of the prion protein (PrP) (*23*). However, the packing arrangement of the β-sheets within the protofilament has yet to be resolved.

Magnetic alignment of fibers has been used to align a number of proteins including silk, keratins, and muscle fibers, and the orientation of these molecules has been attributed predominantly to the diamagnetic anisotropy of the planar peptide bond (*24*). In β-pleated sheets, the planar groups of the peptide bonds are oriented parallel to the sheets, and the axis of smallest diamagnetism is parallel to the pleats, whereas in α-helices, the planar bonds are oriented parallel to the helix axis (*24*). The magnetic field acts upon the existing protein structure and allows orientation of the molecules relative to the magnetic field. Amyloid fibrils align parallel to the magnetic field due to the β-sheet structure. The magnetic force is unlikely to alter the structure of the fibril, but allows arrangement of the fibrils relative to one another.

X-ray diffraction from transthyretin amyloid, which is deposited in familial amyloidotic polyneuropathy (FAP), has also revealed a cross-β fiber diffraction pattern (*21*, *22*). From this high-resolution data, a protein backbone model of the structure of the protofilament subunit was constructed (*21*). The model proposes that the amyloid protofilament is composed almost entirely of β-sheet structure, containing four β-sheets which twist around a central axis. Fiber diffraction of amyloid fibrils of immunoglobulin amyloid, apolipoprotein A1 amyloid, lysozyme amyloid, and others revealed that a similar model could be proposed for these amyloid fibrils, even though each contains unique constituent proteins (*22*).

In the current study, we show that Aβ amyloid fibrils assembled in the presence of a strong magnetic field form a semicrystalline arrangement which yields three-dimensional diffraction data. The properties of these samples fall between that of a cylindrical symmetric fiber and a single crystal, which makes them amenable to more rigorous crystallographic analysis. Using the powerful single-crystal technique of molecular replacement, we have solved the structure of an Aβ peptide fiber, residues 11−25, which is considered to be a core domain within the Aβ amyloid fibril (*8*, *11*, *18*, *25*). Here we describe an atomic resolution model of Alzheimer's amyloid, and this represents significant advance in the structural information. This new insight into the structure of amyloid will allow the natural progression toward the structure of amyloid fibrils formed from full-length Aβ.

EXPERIMENTAL PROCEDURES

Peptide Synthesis and Preparation of X-ray Diffraction Samples. A peptide corresponding to residues 11−25 of the Aβ (NH2-EVHHQKLVFFAEDVG-COOH) was synthesized, purified by reversed-phase HPLC, and lyophilized as previously described (*26*). The Aβ(11−25) peptide was dissolved in water at a concentration of 20 mg/mL and magnetically aligned samples were prepared for X-ray diffraction analysis using standard methodology (*18*, *27*).

Modeling of Aβ(11−25) Peptide. Modeling the Aβ(11−25) structure was performed using the computer graphics program QUANTA (Molecular Simulations) run on a Silicon Graphics workstation. An antiparallel β-hairpin was constructed from a poly-alanine sequence, which was used as a template to insert the side chains corresponding to the Aβ-(11−25) sequence. Both β-hairpin models were energy minimized using CHARMM (*28*) (50 cycles of Steepest Descents) to ensure ideal stereochemistry.

X-ray Fiber Diffraction Data Collection. Data were collected using a wavelength of 0.9515 Å [European Synchrotron Research Facility (ESRF) in Grenoble, France] on a MAR research image plate detector (300 mm diameter) as previously described (*22*). The specimen was initially mounted with the major fiber axis normal to the incident X-ray beam with near zero tilt. This was achieved by rotating the sample until the intensity of the reflections above and below the equator were symmetrical. Additional fiber patterns were collected using a rotating anode (CuKα, wavelength = 1.5418 Å) equipped with a MAR research image plate (diameter 180 mm). Patterns were collected at rotations of 90°, parallel to the axis of the fiber and at right angles to the initial direction. A low angle pattern was collected on photographic film, with a specimen to film distance of 289.4 mm using a rotating anode CuKα source.

Data Processing of Fiber Patterns. Measurements of the reflection spacings in the patterns were made using IPDISP (*29*) from which several cell parameters were derived. Using the CCP13 suite of programs (http://wserv1.dl.ac.uk/SRS/CCP13/) as described in documentation, the specimen to film distance, center, tilt, and rotation of the patterns were calculated using FIX. FTOREC was used to convert the pattern to reciprocal space coordinates and to quadrant average the pattern. LSQINT was subsequently utilized to input various cells and space groups using profile parameters (*30*) and to optimize the spread of the predicted reflections in reciprocal angstroms and degrees. These parameters were used to predict reflections for a particular unit cell and space group, with the optimized spread widths, and the background was subtracted from the patterns using the Roving window

method. Intensities were fitted using maximum entropy algorithms, and the accuracy of the fit was measured by the output *R*-factor and by comparison of the calculated and observed diffraction pattern images. When optimized, the final intensities were fitted and a list of *hkl* with corresponding integrated intensity was generated.

Molecular Replacement Using a Modeled β-Hairpin as a Starting Model. LSQINT (http://wserv1.dl.ac.uk/SRS/CCP13/) outputs Lorentz-corrected intensities from which structure factor amplitudes were calculated (*29*). All integrated reflections were used for molecular replacement. A rotation search was performed using X-plor (*31*) and parameters such as vector length and resolution were altered in the rotation function to arrive at a consistent solution. The solutions were put in order of correlation using Patterson Correlation Coefficient refinement. The optimum rotation solutions were submitted to translation search, in order locate the model coordinates in the unit cell. A translation factor, packing function, and *R*-factor were recorded and new coordinates inspected using the graphics program "O" (*32*). The viability of the solution was assessed by examination of symmetry related objects on a Silicon graphics workstation. Structure factors were calculated from model coordinates using CCP4 programs, and diffraction diagrams were viewed and compared to observed diffraction patterns using Hklview and Ipdisp (*29*).

Refinement of the Model Solution. The proposed model was improved by running 40 cycles of rigid-body refinement in X-plor (*31*) to shift the peptide into a more structurally favorable position. The new coordinates were examined on a Silicon graphics work station using the graphics program O (*32*).

RESULTS

Selection of a Model Amyloid-Forming Peptide. The peptide corresponding to residues 11−25 of Aβ was carefully chosen based upon its similar characteristics to full-length Aβ and because it is a key sequence that maintains the structural integrity of the fiber. This peptide forms amyloid fibrils in vitro which resemble those of full-length Aβ(1−40) and Aβ(1−42) (*8*, *11*) and ex-vivo amyloid (*17*). They are known to be particularly well-ordered fibrils which have been shown to give highly oriented diffraction patterns (*18*). Regions of this peptide have been suggested to be important in conformation switching from α- to β- structure, particularly histidine residues 13 and 14 and glutamate residues 11 and 22. It has been hypothesized that the electrostatic character of these residues leads to salt-bridge formation and facilitates β-sheet folding and fibrillogenesis (*8*, *11*, *33*). Single amino acid substitutions of various residues in this region (residues, 16, 18, 19, 20) result in a decreased propensity for fibril formation, suggesting that these residues are particularly important for amyloid fibril formation (*8*, *12*, *26*, *34*). The Dutch-type mutation, Glu22Gln, is known to increase fibril formation and stability of the peptide (*27*, *35*, *36*). The peptide contains a hydrophobic cluster of residues at 17−21 which has been proposed to be involved in important side-chain interactions (*11*, *27*, *37*). Recently, it has been shown that the shortest peptide capable of forming fibrils is 14−23 (*25*), which represents the core of our structural model. The peptide sequence, KLVFF (residues 16−20), has been shown to behave as an inhibitor of amyloid fibril formation, indicating the importance of these residues in the assembly process (*38*).

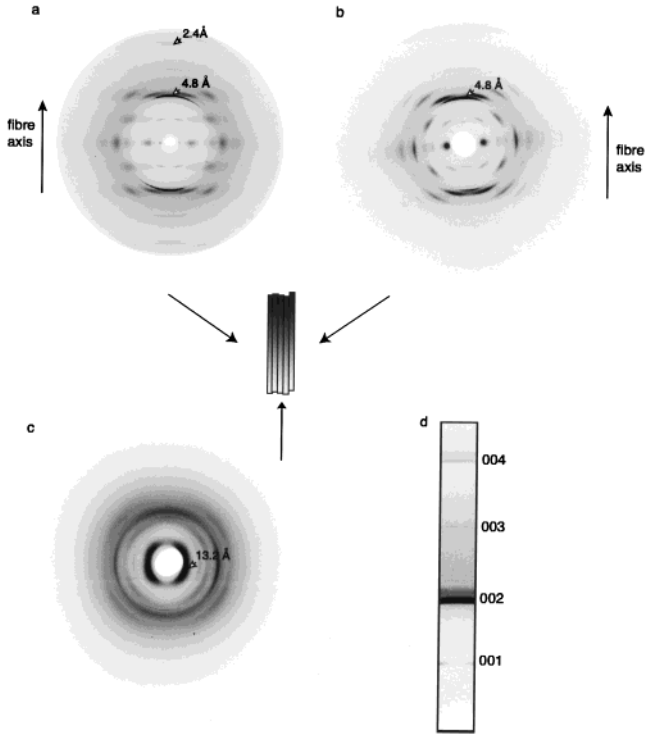

FIGURE 2: Three wide angle diffraction patterns taken from the magnetically aligned Aβ(11−25) fiber specimen. Images a and b are taken at right angles to the fiber axis and at 90° to one another and both show the sharp, strong, meridional reflection at 4.8 Å. Image c is taken down the axis of the fiber and shows a reflection at 13.2 Å spacing on the equator as well as very intense 10−11 Å reflections. Image d shows a slice of diffraction pattern a, showing the four meridional reflections which index to *hkl* = 001, 002, 003, and 004 highlighting that *hkl* = 001 and 003 are much less intense than 002 and 004.

X-ray Fiber Diffraction from Magnetically Aligned Amyloid Fibrils. The crystalline nature of the oriented fibrils allowed us to sample data from three crystallographic zones that resulted in three distinct wide angle patterns (Figure 2). Sampling from the two directions perpendicular to the fiber (Figure 2, panels a and b) exhibit the classic reflections of a cross-β pattern consisting of an extremely strong and sharp 4.8 Å reflection on the meridian (corresponding to hydrogen bond spacing along the fiber axis) and more diffuse reflections at 10−11 Å on the equator (corresponding to the intersheet spacing). In addition, Bragg reflections on layer lines were observed with a spacing of 9.6 Å, which was interpreted as corresponding to the spacing of antiparallel β-strands. Diffraction patterns (Figure 2, panels a and b) taken from the specimen at 90° rotation around the fiber axis direction showed a variation in the radii of reflections and when tilted by 90° (i.e., the direction down the fiber axis) defined arcs rather than the expected rings were observed (Figure 2c). This pattern showed the strong 10.7 Å reflections (horizontal axis) and also a weaker, sharper reflection at 13.2 Å (Figure 2c). The presence of arcs suggests that, unlike a typical cylindrical fiber, the specimen is not circularly symmetric and has preferred orientation. This is consistent with a semicrystalline order in both the hydrogen-bonding and intersheet directions. Additional data was collected by

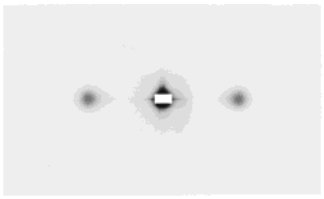

FIGURE 3: Low-angle diffraction pattern taken from the magnetically aligned Aβ(11−25) peptide specimen. A single reflection is observed on the equator at 44.2 Å.

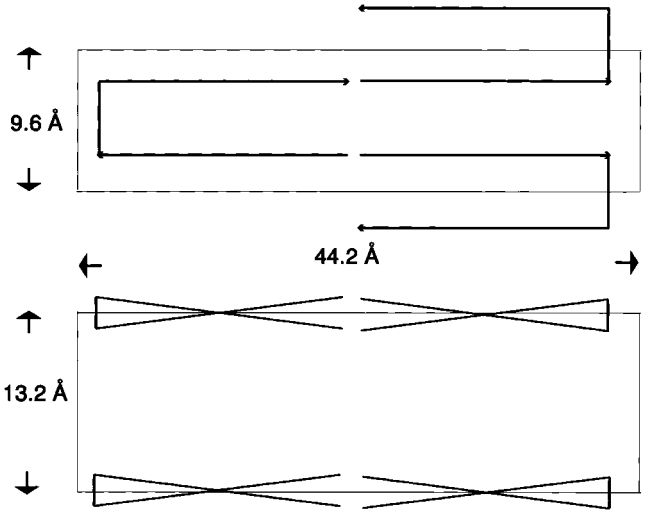

FIGURE 4: Schematic representing the contents predicted for the unit cell $a = 44.2$ Å, $b = 13.2$ Å, $c = 9.6$ Å, $\alpha = 90°$, $\beta = 90°$, $\gamma = 90.1°$. The β-hairpin is represented by the solid black lines and the cell by the fine lines.

low-angle fiber diffraction of the Aβ(11−25) specimen, which revealed a single equatorial reflection on the equator at 44.2 Å (Figure 3). This reflection is representative of the long-range order within the peptide fibril, such as the boundaries of the constituent protofilaments.

For convenience in processing, the *c* axis was indexed to the meridian of the pattern, which corresponds to the long fiber axis (*Z*). A weak reflection was observed on the meridian at 9.6 Å, which was assigned to the *c* direction of the unit cell. Cell axis *a* was taken to be 44.2 Å based on the low-angle equatorial reflection (Figure 3). Sampling down the fiber showed sharp 13 Å arced reflections and this direction was assigned as the *b* axis. On this basis, the unit cell parameters were deduced to be $a = 44.2$, $b = 13.2$, $c = 9.6$ (illustrated schematically in Figure 4).

The mirror symmetry of all three zones from the specimen (symmetry about meridionals and equatorials) suggests that the space group symmetry is orthorhombic or monoclinic with γ near 90°. The volume that would be taken up by a fifteen residue peptide folded into a hairpin is ∼2300 Å^3 and the volume of the predicted cell is 5600 Å^3 (*38*). Therefore, there is sufficient space for only two asymmetric units in the unit cell. The $P2_1$ symmetry restrictions state, $l = 2n$, and the pattern exhibits a meridional at $l = 1$, suggesting that the lattice is pseudo-symmetrical. This would explain why the 001 and 003 reflections are considerably weaker than the much more intense 002 and 004 (Figure 2d). The pseudo spacegroup of $P2_1$ would produce a 2/1 helix (2 units/turn). Upon the basis of these findings the unique axis was assigned to *c* with the γ angle near to 90° (space group $P112_1$, 1004; crystallographic tables, volume 1) (Figure 4).

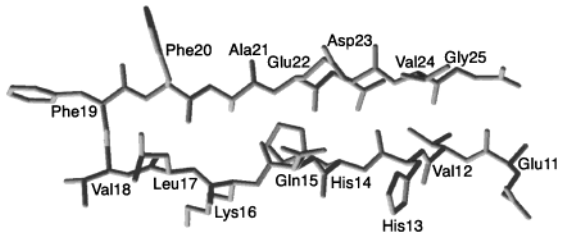

FIGURE 5: Model of the β-hairpin of Aβ(11−25) with labeled amino acid side-chains. The fifteen residue peptide was modeled as a type-I β-hairpin, with seven residues in each β-strand. The figure was generated from the coordinates using Molscript (*47*).

Modeling of the Aβ(11−25) β-Hairpin. A model corresponding to the sequence of Aβ(11−25) was devised, and constructed from an initial poly-alanine template (Figure 5). The strands contained seven residues separated by a type I β-turn and measure about 22 Å in length. The distance between the strands in the hairpin was 4.8 Å in the center and the strands twist relative to one another as is energetically favorable in a β-sheet (*40*). The structure was minimized using CHARMM (*28*) to ensure reasonable stereochemistry. This structural model was used as a search model (Figure 5).

Molecular Replacement. Lorentz-corrected intensities output from the CCP13 programs (http://wserv1.dl.ac.uk/SRS/CCP13/) were converted to structure factors and the proposed β-hairpin (Figure 5) was used as a search model in molecular replacement routine. The translation function produced a single viable model with minimum clashes and a peak of 2.3σ above the mean for the alanine only model and 2σ above the mean for the β-hairpin model with side chains. Both models produced very similar solutions and following rigid body refinement the *R*-factors reduced by 5%.

A Model of a Magnetically Aligned Amyloid Fibril. The final molecular replacement solution indicated that the β-hairpin structure is positioned in the center of the cell such that the symmetry related pair generates a molecule rotated by 180 ° parallel to *z* and shifted up or down by a half-cell. Structure factors were calculated from these coordinates and simulated diffraction diagrams (*hk*0, *h*0*l*) revealed patterns close to the observed diffraction patterns (data not shown). A model was generated by imposing $P112_1$ symmetry on the molecular replacement solution (Figure 6) and this revealed an arrangement of β-hairpins which form continuous β-sheets. In this arrangement, the β-strand of one hairpin forms a pseudo-continuous β-strand with a strand of the next (see Figure 6). The β-strands are hydrogen bonded by both inter- and intrahairpin interactions and the spacing between β-strands is 4.8 Å. The β-strands are arranged such that they are exactly perpendicular to the fiber axis. The view down the β-sheets shows a spacing between them of around 10−13 Å and the packing arrangement shows that the sheets are staggered relative to one another. The result is striking since it generates continuous β-sheet structure, composed of flat β-sheets, with β-strands arranged antiparallel to one another (Figure 6). The model is consistent with the observation of a cluster of hydrophobic residues (*17*−*21*) which may be important in hydrophobic interactions between molecules.

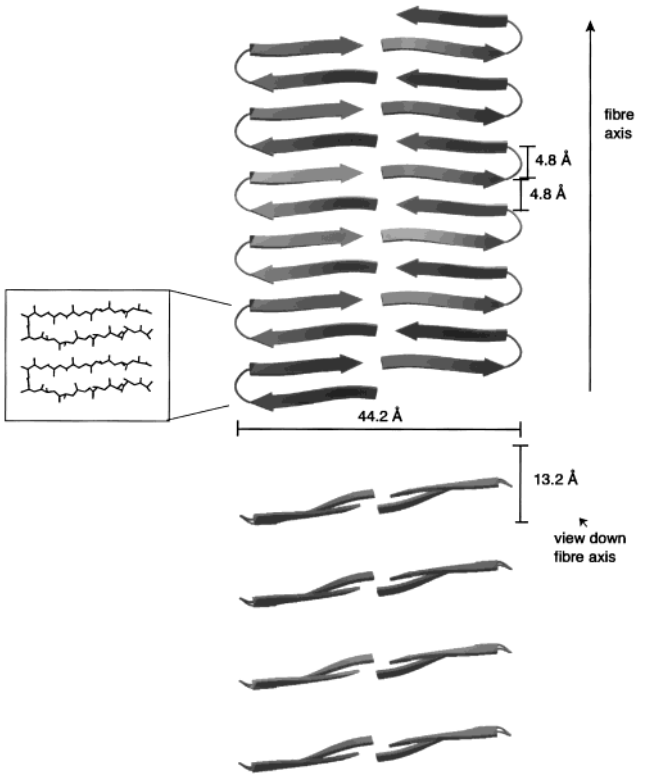

FIGURE 6: Final model of the β-hairpin arrangement within the semicrystalline amyloid specimen. Top panel shows the view of the fiber axis where β-strands are hydrogen bonded to form an elongated β-sheet. The bottom panel is the view down the fiber axis, showing the β-sheets spacing. The inset shows the atomic coordinates of peptide (side chains not shown). The figure was generated from the coordinates using Molscript (*47*).

It is also consistent with the suggested electrostatic interactions between His13 and 14 and Glu22 occurring between β-sheets (*8*, *11*, *33*).

DISCUSSION

Analysis from X-ray data provides information about the structure within a protofilament. A previous model of an amyloid protofilament constructed using fiber diffraction data describes a twisting of the β-strands (*21*). This would be consistent with most globular proteins which usually display a slight twist between adjacent β-strands (*40*). Our final molecular model of amyloid-β assemblies formed in a magnetic field does resemble the model proposed for the TTR amyloid protofilament (*21*). In both instances, the β-strands are aligned perpendicular to the fiber axis and the intersheet and interstrand distances are 10−13 and 4.8 Å, respectively. However, the sheets do not twist in a helical manner but the crystalline arrangement of the β-sheets results in long-range ordering of the β-sheets both in the intersheet direction and the hydrogen bonding direction. This has enabled us to make use of the improved data and information observed from this semicrystalline specimen. This phenomenon may have resulted from the preparation of the polymerizing peptide in a strong magnetic field, which induces an increased ordering of the β-strands relative to one another. However, this is unlikely as alignment of comparable Aβ11−25 amyloid fibrils using a stretch frame (see refs *21* and *22*) produced similar diffraction patterns, although lacking the preferred orientation (Serpell, unpublished results).

Aβ11−25 has served as an ideal peptide for alignment and collection of highly oriented diffraction patterns. The absence of the hydrophobic C-terminal region may have allowed the superior diffraction data to be obtained. Although, it is possible that this peptide forms fibrils that differ slightly from full-length fibrils, we feel that this is a significant contribution to the understanding of amyloid structure. It is probable that the core structure of the protofilaments of amyloid fibrils are similar, while the peripheral structure may differ. The model we present is likely to be very close to a core structure of full-length Aβ amyloid fibrils.

The structure of amyloid protofilaments has been previously investigated using X-ray fiber diffraction and solid-state NMR. Fiber diffraction from aligned Aβ peptide fragments (*18*, *19*) has shown the characteristic cross-β reflections as well as some Bragg spacing along layer lines. Interpretation of these patterns has led to a model in which the fiber is a hollow cylinder or tube composed of five or six "β-crystallites". Each crystallite is made up of approximately five β-sheets separated by 10 Å with the strands containing an estimated six residues (*18*). With this interpretation, the equatorial reflections were found to index to a one-dimensional lattice (*18*) which can be explained by a cylindrical lattice. In our current study, sampling of magnetically aligned Aβ(11−25) in three-dimensions has shown a preferred orientation not previously noted, which indicates that the peptide maybe more appropriately modeled by a semicrystalline lattice. We suggest that rather than being composed of discrete cylinders, we have a crystalline arrangement of β-sheets. Inouye et al. (*18*) propose a cell not unlike ours although containing only two residues of a β-sheet. We suggest that the structure can be modeled by a larger cell which encompasses the entire β-hairpin. We observed a low angle reflection on the equator at 44.2 Å, which we interpret to be the cell length along the polypeptide chain, and that this would contain two hairpins, each measuring about 22 Å length.

Benzinger and co-workers (*41*, *42*) have recently solved the structure of the Aβ(10−35) fragment from solid state NMR. They demonstrated that these selectively ^{13}C-labeled residues exhibited an intermolecular separation of only ∼5 Å which is consistent with a parallel arrangement of the β-strands. One of the most likely explanations for these seemingly contradictory results, is that these unique peptides may differ in their fold. It is conceivable that the Aβ(10−35) peptides assembles into fibrils organized in a parallel arrangement, while the Aβ(11−25) used in our investigation has an antiparallel preference. This may result from differences in the amphipathic characteristics of the individual peptides which, as noted by Soreghan and co-workers (*43*), has a significant effect on fibrillogenesis.

Support for an antiparallel arrangement within other Aβ peptides has been provided by Lansbury et al. (*44*) who also used solid-state NMR to examine the structure of an Aβ-(34−42) fragment which forms sheetlike fibers (*11*, *45*) that are very insoluble. They suggest that the data are inconsistent with hairpins making up the structure, but suggest an antiparallel arrangement of β-strands (*44*). In the case of this short peptide, it is unlikely that a hairpin would be formed from only eight residues, where as the 15 residue length of Aβ(11−25) is rather long for an extended β-strand. Our

diffraction studies and those of others (*7*, *18*, *19*, *27*) have shown a first-order reflection at 9.6 Å which is thought to arise from an antiparallel arrangement of β-strands (true repeat every other β-strand). As discussed, the symmetry of our structure would result in an inherent reduction in intensity (or absence) of the meridional reflection at 9.6 Å (due to the crystallographic absences described in the crystallographic tables for $P2_1$ symmetry). Fiber diffraction from several different ex-vivo amyloid fibrils does not show a meridional reflection at 9.6 Å (*22*). This may be due to the fact that it is not possible to produce well-aligned specimens of ex vivo amyloid and this leads to only the strongest reflections being observed. The absence of this diagnostic antiparallel reflection would be consistent with our observation that even for the magnetically aligned specimen, the 9.6 Å reflection is relatively weak. However, the possibility of a parallel arrangement of β-strands in some amyloid fibrils cannot be ruled out (see ref *21*).

The Aβ(11−25) peptide is known to be a critical domain within Aβ and has been shown to be a key sequence for fibrillogenesis (*38*, *46*). The fiber diffraction patterns obtained from a semicrystalline amyloid specimen allowed interpretation that has led to an atomic model of Alzheimer's disease amyloid. This structure shows similarities to previously described models (*21*, *22*). In this paper, we have described the first level of structure of the Alzheimer's amyloid fibrils, the arrangement of the polypeptide chains within the protofilaments. This is an important first step in constructing a complete model of the full-length Aβ amyloid fibril and this new information will aid understanding the structural mechanisms involved in fibrillogenesis as well as indicating a means of intervention to inhibit amyloid fibril deposition.

ACKNOWLEDGMENT

The authors would like to thank Dr. B. Rasmussen and co-workers for help with data collection at ESRF France, Dr. J. Harford for collection of low-angle diffraction data at Imperial College, London, and Dr. R. Denny for help and guidance with data processing.

REFERENCES

1. Selkoe, D. J. (1991) *Neuron 6*, 487−498.
2. Hardy, J. (1997) *Proc. Natl. Acad. Sci. U.S.A. 94*, 2095−2097.
3. Pike, C. J., Burdick, D., Walencewicz, A. J., Glabe, C. G., and Cotman, C. W. (1993) *J. Neurosci. 13*, 1676−1687.
4. Lorenzo, A., and Yankner, B. A. (1994) *Proc. Natl. Acad. Sci. U.S.A. 91*, 12243−12247.
5. Games, D., Adams, D., Allessandrini, R., Barbour, R., Berthelette, P., Blackwell, C., Carr, T., Donaldson, T., Clemens, J., Gillespie, F., Guilo, T., Hagopian, S., Johnson-Wood, K., Khan, K., Lee, M., Leibowitz, P., Leiberburg, I., Little, S., Masliah, E., McConlogue, L., Montoya-Zavala, M., Mucke, L., Paganini, L., Penniman, E., Power, M., Schenk, D., Seubert, P., Synder, B., Soriano, F., Tan, H., Vitale, J., Wadswoorth, S., Wolozin, B., and Zhao, J. (1995) *Nature 373*, 523−527.
6. Serpell, L. C., Sunde, M., Fraser, P. E., Luther, P. K., Morris, E., Sandgren, O., Lundgren, E., and Blake, C. C. F. (1995) *J. Mol. Biol. 254*, 113−118.
7. Fraser, P. E., Duffy, L. K., O'Malley, M. B., Nguyen, J., Inouye, H. H., and Kirschner, D. A. (1991) *J. Neurosci. Res. 28*, 474−485.
8. Kirschner, D. A., Inouye, H., Duffy, L. K., Sinclair, A., LInd, M., and Selkoe, D. J. (1987) *Proc. Natl. Acad. Sci. U.S.A. 84*, 6953−6957.
9. Lansbury, P. T. (1999) *Proc. Natl. Acad. Sci. U.S.A. 96*, 3342−3344.
10. Lomakin, A., Chung, D. S., Benedek, G. B., Kirschner, D. A., and Teplow, D. B. (1996) *Proc. Natl. Acad. Sci. U.S.A. 93*, 1125−1129.
11. Fraser, P. E., Nguyen, J. T., Surewicz, W. K., and Kirschner, D. A. (1991) *Biophys J. 60*, 1190−1201.
12. Soto, C., Castano, E., Frangione, B., and Inestrosa, N. (1995) *J. Biol. Chem. 270*, 3063−3067.
13. Shen, C.-L., and Murphy, R. M. (1995) *Biophys. J. 69*, 640−651.
14. Stricht, H., Bayer, P., Willbold, D., Dames, S., Hilbich, C., Beyreuther, K., Frank, R., and Rosch, P. (1995) *Eur. J. Biochem. 233*, 293−298.
15. Coles, M., Bicknell, W., Watson, A., Fairlie, D., and Craik, D. (1998) *Biochemistry 37*, 11064−11077.
16. Shao, H., Jao, S., Ma, J., and Zagorski, M. (1999) *J. Mol. Biol. 285*, 755−773.
17. Kirschner, D., Abraham, C., and Selkoe, D. (1986) *Proc. Natl. Acad. Sci. U.S.A. 83*, 503−507.
18. Inouye, H., Fraser, P., and Kirschner, D. (1993) *Biophys. J. 64*, 502−519.
19. Malinchik, S., Inouye, H., Szumowski, K., and Kirschner, D. (1998) *Biophys. J. 74*, 537−545.
20. Geddes, A. J., Parker, K. D., Atkins, E. D. T., and Beighton, E. (1968) *J. Mol. Biol. 32*, 343−358.
21. Blake, C., and Serpell, L. (1996) *Structure 4*, 989−998.
22. Sunde, M., Serpell, L., Bartlam, M., Fraser, P., Pepys, M., and Blake, C. (1997) *J. Mol. Biol. 273*, 729−739.
23. Inouye, H., and Kirschner, D. A. (1997) *J. Mol. Biol 268*, 375−389.
24. Worcester, D. (1978) *Proc. Natl. Acad. Sci. U.S.A. 75*, 5475−5477.
25. Tjernberg, L., Callaway, D., Tjernberg, A., Hahne, S., Lilliehook, C., Terenius, L., Thyberg, J., and Norstedt, C. (1999) *J. Biol. Chem. 274*, 12619−12625.
26. Fraser, P. E., McLachlan, D. R., Surewicz, W. K., Mizzen, C. A., Snow, A. D., Nguyen, J. T., and Kirschner, D. A. (1994) *J. Mol. Biol. 244*, 64−73.
27. Fraser, P. E., Nguyen, J. T., Inouye, H., Surewicz, W. K., Selkoe, D. J., Podlisny, M. B., and Kirschner, D. A. (1992) *Biochemistry 31*, 10716−10723.
28. Brooks, B., Bruccoleri, R., Olafson, B., States, D., Swaminathan, S., and Karplus, M. (1983) *J. Comp. Chem. 4*, 187−217.
29. CCP4. (1994) *Acta Crystallogr., Sect. D 50*, 760−763.
30. Fraser, R. D. B., Macrae, T. P., Miller, A., and Rowlands, R. J. (1976) *J. Appl. Crystallogr. 9*, 81−94.
31. Brunger, A. (1987) *Xplor. Version 3.1: A System for X-ray Crystallography and NMR*, Yale University Press, New Haven and London.
32. Jones, T. A., Za, Y.-Y., Cowan, S. W., and Kjeldgaard, M. (1991) *Acta Crystallogr., Sect. A 47*, 110−119.
33. Zagorski, M., and Barrow, C. (1992) *Biochemistry 31*, 5621−5631.
34. Hilbich, C., Kisters-Woike, B., Reed, J., Masters, C., and Beyreuther, K. (1991) *J. Mol. Biol. 218*, 149−163.
35. Levy, E., Carman, M., Fernadez-Madrid, I., Lieberburg, I., Poser, M., Van Duinen, S., Bots, G., Luyendijk, W., and Frangione, B. (1990) *Science 248*, 1124−1126.
36. Wisniewski, T., Ghiso, J., and Frangione, B. (1991) *Biochem. Biophys. Res. Commun. 179*, 1247−1254.
37. Zhang, S., Casey, N., and Lee, J. (1998) *Folding Des. 3*, 413−422.
38. Tjernberg, L. O., Naslund, J., Lindqvist, F., Johansson, J., Karlstrom, A. R., Thyberg, J., Terenius, L., and Nordstedt, C. (1996) *J. Biol. Chem. 271*, 8545−8548.
39. Matthews, B. W. (1968) *J. Mol. Biol. 33*, 491−497.
40. Chothia, C. (1973) *J. Mol. Biol. 75*, 295−302.

41. Benzinger, T., Gregory, D., Burkoth, T., Miller-Auer, H., Lynn, D., Botto, R., and Meredith, S. (1998) *Proc. Natl. Acad. Sci. U.S.A. 95*, 13407−13412.
42. Benzinger, T. L. S., Gregory, D. M., Burkoth, T. S., Miller-Auer, H., Lynn, D. G., Botto, R. E., and Meredith, S. C. (2000) *Biochemistry 39*, 3491−3499.
43. Soreghan, B., Kosmoski, J., and Glabe, C. (1994) *J. Biol. Chem. 269*, 28551−28554.
44. Lansbury, P. T., Costa, P. R., Griffiths, J. M., Simon, E. J., Auger, M., Halverson, K. J., Kocisko, D. A., Hendsch, S. S., Ashburn, T. T., Spencer, R. G. S., Tidor, B., and Griffin, R. G. (1995) *Nat. Struct. Biol. 2*, 990−998.
45. Halverson, K., Fraser, P., Kirschner, D., and Lansbury, P. J. (1990) *Biochemistry 29*, 2639−2644.
46. Findeis, M. A., Musso, G. M., Arico-Muendel, C. C., Benjamin, H. W., Hundal, A. M., Lee, J., Chin, J., Kelley, M., Wakefield, J., Hayward, N., and Molineaux, S. M. (1999) *Biochemistry 38*, 6791−6800.
47. Kraulis, P. (1991) *J. Appl. Crystallogr. 24*, 946−950.
48. Serpell, L. C., Sunde, M., Benson, M. D., Tennent, G. A., Pepys, M. A., and Fraser, P. E. (2000) *J. Mol. Biol. 300*, 1033−1039.

BI000637V